Near-microsecond human aquaporin 4 gating dynamics in static and alternating external electric fields: Non-equilibrium molecular dynamics

Niall J. English[1,a)] and José-A. Garate[2,3]
[1]*School of Chemical and Bioprocess Engineering, University College Dublin, Belfield, Dublin 4, Ireland*
[2]*Computational Biology Laboratory, Life Sciences Foundation, Santiago, Chile*
[3]*Centro Interdisciplinario de neurociencia de Valparaiso, Universidad de Valparaiso, Valparaiso, Chile*

(Received 19 April 2016; accepted 3 August 2016; published online 25 August 2016)

An extensive suite of non-equilibrium molecular-dynamics simulation has been performed for ~0.85-0.9 μs of human aquaporin 4 in the absence and presence of externally applied static and alternating electric fields applied along the channels (in both axial directions in the static case, taken as the laboratory z-axis). These external fields were of 0.0065 V/Å (r.m.s.) intensity (of the same order as physiological electrical potentials); alternating fields ranged in frequency from 2.45 to 500 GHz. In-pore gating dynamics was studied, particularly of the relative propensities for "open" and "closed" states of the conserved arginines in the arginine/aromatic area (itself governed in no small part by external-field response of the dipolar alignment of the histidine-201 residue in the selectivity filter). In such a manner, the intimate connection of field-response governing "two-state" histidine states was established statistically and mechanistically. Given the appreciable size of the energy barriers for histidine-201 alignment, we have also performed non-equilibrium metadynamics/local-elevation of static fields applied along both directions to construct the free-energy landscape thereof in terms of external-field direction, elucidating the importance of field direction on energetics. We conclude from direct measurement of deterministic molecular dynamics in conjunction with applied-field metadynamics that the *intrinsic* electric field within the channel points along the +z-axis, such that externally applied static fields in this direction serve to "open" the channel in the selectivity-filter and the asparagine-proline-alanine region. *Published by AIP Publishing.* [http://dx.doi.org/10.1063/1.4961072]

INTRODUCTION

Aquaporins (AQPs) constitute an extensive family of trans-membrane proteins forming channels which conduct selectively water, as well as other small uncharged molecules (such as glycerol). This selective permeation is as a result of osmotic pressure between both sides of the membrane, serving also to exclude very strictly the passage of ions and protons.[1,2] AQPs are in all known lifeforms and are essential for regulating precisely water content in organs and cells. In humans, their defective function is implicated in various pathological conditions, such as nephrogenic diabetes, insipidus, and congenital cataracts.[3] Since their original discovery by Agre *et al.*,[4] several hundred AQPs have been elucidated and characterised.[3,5] A more complete understanding of osmotically driven water permeabilities and fluxes in AQPs is essential for progress in medical research, to establish more confidently their function and their potential involvement in medical conditions. Bearing this in mind, water fluxes in AQPs are estimated relatively routinely, via reconstitution of channels in liposomes and monitoring changes in volume due to concentrations of an impermeable solute; it may also be possible to estimate diffusive permeability from isotope labelling.[1,2,4,6–8] To obtain single-channel permeabilities, knowing AQP density is essential, i.e., the liposome's precise lipid-to-protein composition—in most cases, a significant challenge.

Even knowing channel densities, obtaining an atomistic-level description of water-transport mechanisms in AQPs is not experimentally feasible, due primarily to the short, nanosecond timescales involved.[9,10] Given these relatively fast kinetics, and together with recent availability of atomic-resolution AQP structures,[11–13] molecular dynamics (MD) has become a very valuable tool for gaining theoretical insights into underlying mechanisms.[14–23] In particular, a permeation mechanism has been proposed in which the pore acts as a "two-stage filter"; a "selectivity filter" ("SF") (aromatic/arginine region) at the narrowest part of the channel acts as one, whilst a well-conserved asparagine-proline-alanine (NPA) motif (dubbed "CE") serves as the other, wherein a well-defined water dipolar rotation occurs during passage through the channels.[24] MD studies have considered the characteristics of proton blockage by AQPs,[25–30] the transport of other solutes,[31–34] the gating of aquaporins,[35–37] and aquaporin-mediated cell adhesion.[38]

In particular, Human Aquaporin 4 (h-AQP4) is abundantly expressed in blood-brain and brain-cerebrospinal fluid interfaces and is responsible for homeostasis of cerebral water; its function is related to neuropathological disorders

a)Author to whom correspondence should be addressed. Electronic mail: niall.english@ucd.ie. Tel.: +353-1-7161646. Fax: +353-1-7161177.

like brain edema, stroke, and head injuries.[2,3,39] Recently, the atomic structure of h-AQP4 was resolved by x-ray crystallography at a resolution of 1.8 Å [Protein Data Bank (PDB) entry code 3GD8].[40] As with all AQPs, h-AQP4 forms homo-tetramers in cell membranes, having in each functional unit eight transmembrane helices for which both well-conserved NPA motifs meet at the centre of the pore, while the histidine/arginine selectivity filter is located on the extracellular side. MD and quantum-mechanical simulations suggest that for both the NPA motifs and selectivity filter, electrostatic effects dominate in-channel water orientation.[30]

Given this framework, and considering that recently there has been increasing focus on interaction mechanisms at the basis of biological effects of electromagnetic fields,[41–46] as well as an increasing attention on the use of intense electric fields for a diverse applications, e.g., nanotechnology for bio-sensing,[47] there is great interest in investigating the effect of external electric fields (both static and time-varying) on molecular/water transport in confined geometries (such as nano-pores or aquaporins). For instance, Schoenbach *et al.* have reported the experimental results of electric field of the order of MV/m applied to cells.[48]

Garate *et al.* performed MD simulations of h-AQP4 embedded in a solvated lipid bilayer,[49] and considered the effects of continuously applied static and alternating electric fields on water transport process, and key features such as single-channel osmotic and diffusive permeabilities. Reale *et al.* carried out similar simulation of embedded-bilayer h-AQP4, albeit in the absence and presence of nanosecond-scale static and alternating electric-field impulses, together with post-field relaxation,[50] establishing, with the aid of in-field metadynamics, that the dipolar alignment of histidine-201 plays an intimate role in determining gating mechanisms and water flux. Moreover in previous work aside from h-AQP4,[49,50] Garate *et al.* observed that water flux through single walled carbon nanotubes (SWCNTs) embedded in solvated lipid membranes is affected by low-intensity static and time-varying electric fields,[51–53] and the effects of dipolar rotation were noted on modulating water flux.[49–53]

However, intriguing, largely unresolved, open questions remain from the seminal studies of Refs. 49 and 50 in relation to h-AQP4 behaviour in external electric fields. Notably, these include the interplay of the applied fields *vis-à-vis* the *intrinsic local electric field within the pore under normal conditions (the so-called resting potential)*, i.e., a transmembrane potential normally ranging from −80 to −40 mV on the intracellular side with respect to the extracellular side, as well as clarification of free-energy barriers for *histidine-201 dipolar alignment in terms of axial field direction*. Indeed, Ref. 24 discusses, with acuity and insight, the voltage regulation of water permeation through aquaporins (including h-AQP4) by means of judicious placement of ions on either side of the membrane to achieve a *de facto* external trans-membrane potential (as opposed to ones applied formally);[49,50] the identification of the "two-stage" water-permeation mechanism in the arginine/aromatic construction area, and effect of voltage regulation thereon, serves as motivation to unveil the potential subtle "ballet" of external and intrinsic electric fields interacting, including the effect of the axially applied external-field direction.

Bearing especially the subtle matter of voltage regulation in mind, in the present study, we have performed equilibrium and non-equilibrium molecular-dynamics (NEMD) for ∼0.85 -0.9 μs of h-AQP4 in the absence and presence of externally applied static and alternating electric fields applied along the channels (in both axial directions in the static case, taken as the laboratory z-axis). Given the need to achieve good sampling statistics for selectivity-filter- (SF) and NPA (CE) "switching" events (in terms of histidines' 201 and 95 dipolar alignment or "open"-"closed" transitions, and energy barriers governing these events), and the use of time-dependent external fields[45] in some simulations (in the guise of 2.45–500 GHz fields), the need to apply longer-time MD, of the order of a microsecond, is evident. The (r.m.s.) intensity of the applied fields has been considered similar to the one adopted in previous work[49,50] (0.0065 V/Å); in fact, given that such a field intensity produces transmembrane voltages of ∼0.52 V (from ∼80 Å simulation-box length), this is of the order of 6-12 times the trans-membrane potential,[54] i.e., the applied electric fields are of the same general order as the physiological one (which acts axially, *ipso facto*).[24] By changing direction of the (axially applied) static fields, we can study systematically the interplay of intrinsic and external electric fields. Given the relatively low magnitude of the external-field forces on each atom at this intensity *vis-à-vis* those of inter- and intra-molecular potential's interactions (around 1% or less), longer-time MD is also necessary for good statistical sampling in an effort to elucidate external-field effects with good precision. Of course, with in-field metadynamics, applied for the first time (to the knowledge of the authors) in Ref. 50 to study pulsed-field effects on water passage in h-AQP4, using static (time-independent) fields only is *sine qua non* for non-equilibrium (in-field) metadynamics.[45]

METHODOLOGY

The computational methodology is largely identical to that of Garate *et al.*[49] for deterministic (non-equilibrium) MD and to Reale *et al.*[50] for (in-field) metadynamics; however, a brief synopsis is given here. The crystal structure of h-AQP4 was obtained from the Protein Data Bank (www.pdb.org, entry 3GD8),[55] and the tetramer unit constructed using transformation matrices therein. The missing hydrogen atoms were added assuming a pH of 7.5 for the protonation states using the internal coordinates of the CHARMM27 topology;[56,57] histidine protonation states were set at neutral, with the proton positioned on N_δ. pKa calculations were performed; no substantial differences between either protonation states (i.e., Nε and N_δ) were observed. All crystallographic water molecules were retained. The h-AQP4 tetramer was embedded in an equilibrated and solvated palmitoyloleoylphosphatidyl-ethanolamine (POPE) lipid bilayer placed in the x-y plane; overlapping lipids were removed, and a solvation shell of 20 Å was added in the −z and z direction, while the z-axis was set as normal to the bilayer.[49] Na^+ and Cl^- ions were placed randomly in the water to neutralise the system, with final concentration

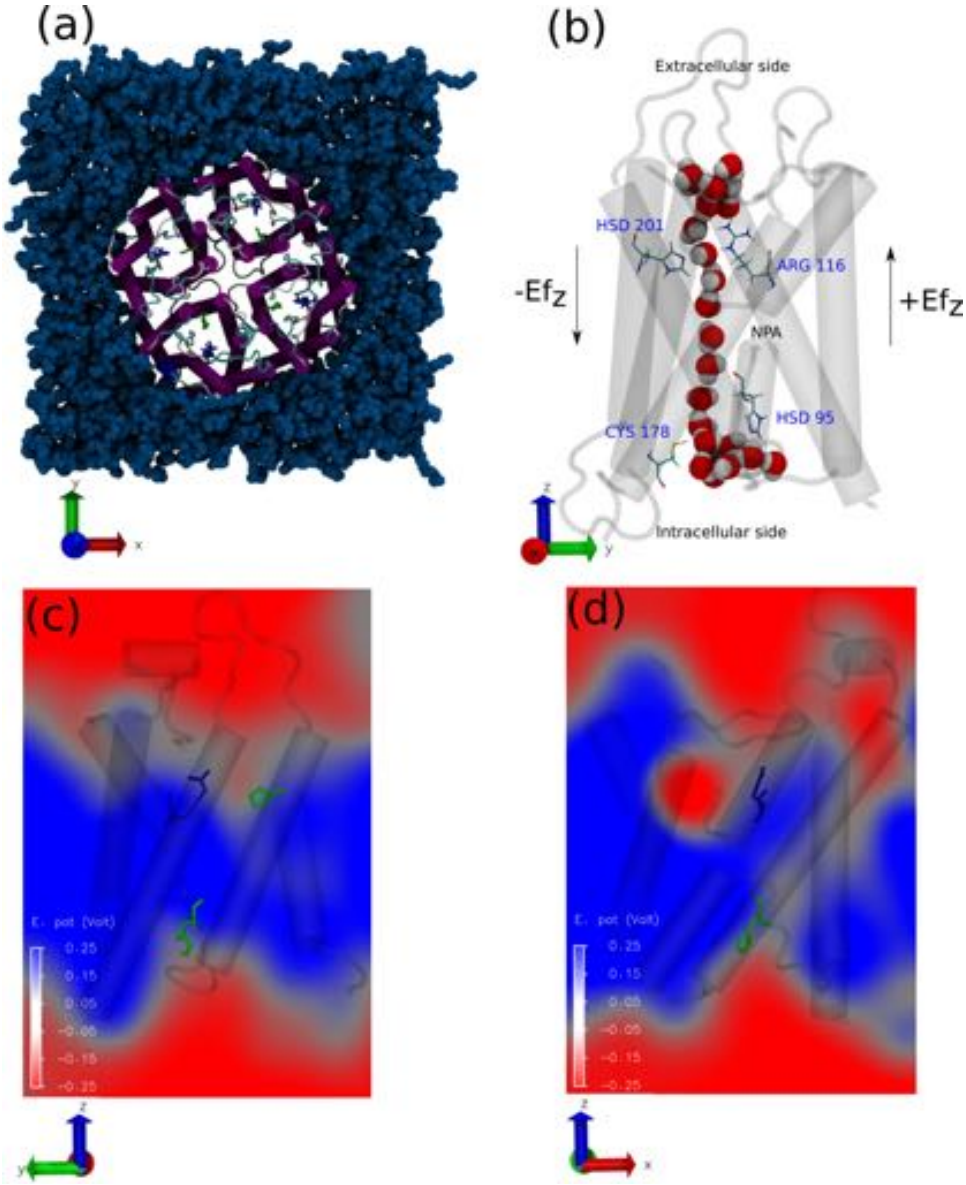

FIG. 1. Simulated system. (a) Top view of the AQP4 tetramer in cartoon representation; (b) side view of a single AQP4 monomer with water within the constriction region of the channel. (c) and (d) Electrostatic potentials centered at the pore along the z-y and z-x planes, respectively. In dark blue, POPE molecules; in blue and green S.F. residues R216 and H201 and H95, respectively; in white, red, cyan, blue, and yellow hydrogen, oxygen, carbon, nitrogen, and sulphur atoms, respectively. HSD, N_δ protonated histidine.

of 50 mM. The final dimensions of the periodic cell were $101 \times 101 \times 80$ Å, consisting of a total of 85 701 atoms.[49] In Fig. 1, a graphical depiction of the simulated system is shown (indicating the +z and −z directions).

All MD simulations were performed with NAMD v2.10[58,59] with the CHARMM27 potential[55] and TIP3P water model.[60] The particle mesh Ewald[61] method was used for long-range electrostatics, with a reversible reference-system propagation algorithm (r-RESPA) multiple time step decomposition[62] of 1, 2, and 4 fs for bonded, short-range non-bonded, and long-range electrostatic interactions, respectively.[49] All production runs were performed with an isothermal-isobaric ensemble (NPT) reservoir (with constant cross-sectional x-y surface area) with set points of 1 atm and 298 K using the Nosé–Hoover method[63] and Langevin dynamics for piston fluctuation control[64] with a 1 ps^{-1} damping coefficient. The SHAKE algorithm[65] was applied to constrain bond lengths to hydrogen atoms. System relaxation is as described in Ref. 49—essentially energy minimisation and equilibration MD.

Approximately 0.85-9 μs of production MD was performed under zero-field, equilibrium conditions, with NEMD (non-equilibrium MD under time-dependent electric fields) simulations of the axially applied fields with (r.m.s.) intensity of 0.0065 V/Å being of the same duration. Static fields were applied[45] along the −z and +z directions (with previous studies[49,50] just considering the −z case). Alternating fields had frequencies of 2.45, 20, 50, 100, 200, and 500 GHz. Equilibrium MD simulation indicates that local electric field intensities in condensed phases are in the range of around 1.5 to 2.5 V/Å,[66,67] giving rise to *de facto* "signal-to-noise" ratios of around 350:1 to 250:1 for the intrinsic to applied fields in the present work. Field strengths in the 0.1-0.5 V/Å range may be obtained routinely in experiment by applications of potentials of 1–5 kV onto tips of radius 10-100 nm.[68] Graphics processing unit (GPU) deployment was used in NAMD v2.10,[69] giving substantial acceleration (approximately 2.5-3-fold) *vis-à-vis* the equivalent number of central processing unit (CPU)-cores on quad-core Intel Xeon nodes connected via sub-microsecond-latency Infiniband.

The acceleration was primarily, though not only, in the evaluation of intermediate-range non-bonded van der Waals and electrostatic interactions.[53,70,71]

In a similar vein to Refs. 24 and 37, we define d_{SF} and d_{CE} which gauge, respectively, the distance between the nitrogen hydrogen-bond acceptor in HIS-201 and the closer terminal nitrogen atom in Arg-216 at the selectivity filter (SF), and the distance between the nitrogen hydrogen-bond acceptor atom of HIS-95 and the sulphur atom in Cys-178 at the CE—see Fig. 2. This allows us to probe two-state gating mechanisms, and external-field effects thereon.

To explore the free-energy landscape and thermodynamics of histidine-201 side-chain configurations and the dependence upon axial field direction, Potentials of

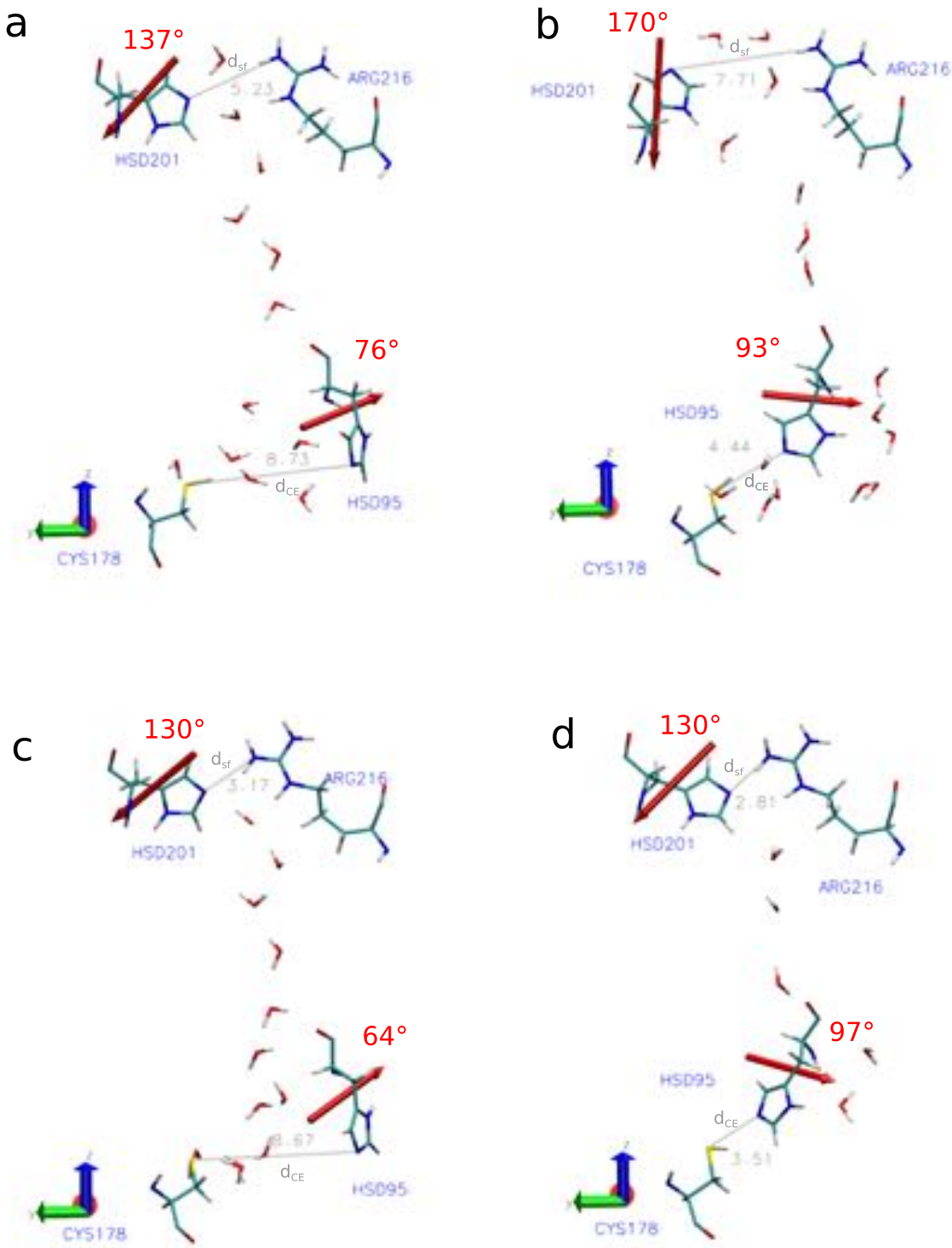

FIG. 2. Examples of the different states observed during simulations. In grey are d_{SF} and d_{CE} distances (in Angstroms). In red, dipole vectors of histidines 95 and 201 are shown, and the corresponding angles with the +z-axis. Panels (a), (b), (c), and (d) show open-open (O-O), open-closed (O-C), closed-open (C-O), and closed-closed (C-C) states, respectively. HSD, N_δ protonated histidine; in white, red, cyan, blue, and yellow are hydrogen, oxygen, carbon, nitrogen, and sulphur, respectively.

Mean Force (PMFs) were derived using the local-elevation method,[72,73] also known as metadynamics, under static electric fields acting along *both* z-directions, albeit at one tenth and one half of the previously applied intensities (i.e., 0.000 65 and 0.003 25 V/Å). Lower intensities were used for metadynamics, as opposed to NEMD, since metadynamics relies on linear scaling with lower field intensity in what has been established already as the linear-response régime of external-field intensity.[66,67] Also, using two (lower) field strengths allows for studying variation of PMF profile *vis-à-vis* the zero-field case[50] to assess the influence of field intensity. In such a way, and in view of the activation-energy barriers identified by direct sampling from free MD,[49,50] the influence of field effects on the orientational-state PMFs may be gauged more precisely, and rough trends with field intensity uncovered. Local-elevation metadynamics constructs stages in which a memory penalty function is applied to a subspace of coordinates $\mathbf{Q}$,[72,73] i.e.,

$$U_{\text{meta}}(\mathbf{Q}) = \sum_{t'=\delta t, 2\delta t, \ldots}^{t'<t} W \prod_{i=1}^{N_{gc}} F(Q_i; d_i). \tag{1}$$

Here, $N_{gc}(\mathbf{Q})$ is the number of generalised coordinates, Q_i, e.g., a set of torsional HIS-201 angles. W and d_i are free parameters, namely, the height and width of each bin, respectively. F denotes a one-dimensional repulsive Gaussian "hill",

$$F(Q_i; d_i) = \exp\left(-\frac{(Q_i(q;t) - Q_i(q;t'))^2}{2\delta_{Q_i}^2}\right) \tag{2}$$

with centres located at previously visited configurations, extending by approximately $2\delta_{Q_i}$ along the Q_i direction. The latter depends parametrically on the bin width, d_i. In general, $U_{\text{meta}}(\mathbf{Q})$ (for a sufficiently long build-up time) is a good approximation of the negative of the free-energy surface or PMF,

$$\text{PMF}(\mathbf{Q}) \approx -U_{\text{meta}}(\mathbf{Q}) + K. \tag{3}$$

Here, K is an arbitrary constant usually defined to set the lowest PMF value to nought. PMF profiles were calculated along the torsion angle $\angle C - C_\alpha - C_\beta - C_\gamma$ under static-field conditions along both z-directions. A penalty potential of the form of Eqs. (1) and (2) was adopted. Further details are described in Ref. 50.

Although the applied fields will have an important polarisation effect at the atomic level, CHARMM27 is a non-polarisable potential, thus the results presented will not account for this effect. Despite this shortcoming, previous works of English *et al.*[66,67,74] have shown that the effects on liquid water under the influence of e/m-fields are described qualitatively compared to the use of a polarisable potential. Apart from the matter of polarisability *per se*, Gumbart *et al.* have shown that the application of external electric fields is valid for a proper description of the membrane potential.[54]

A further point to consider about the relatively low field intensity of 0.0065 V/Å, apart from near-identical level to physiologically trans-membrane electric fields, is that an approximate "threshold" intensity for non-thermal effects corresponds to around 0.01 V/Å for liquid water;[66,67] this agrees with more recent estimates for either static electric or electromagnetic fields affecting solvated proteins (although the latter studies concentrated on local displacements in the protein itself, and variation in local laboratory-frame dipole moment).[42,75] Therefore, 0.0065 V/Å is "at the limit" of what may be reasonably expected to be observed in terms of tangible *athermal* field effects with some degree of statistical confidence from microsecond NEMD. Moreover, these low intensities do not disturb the integrity of the lipid bilayer and protein's structural stability, based on root-mean square deviation (RMSD) calculations.[49]

RESULTS AND DISCUSSION

Typical snapshots of water molecules within the channels and more extreme examples the 2×2 (open/closed, SF and CE) states are shown in Figs. 1 and 2. Further details of the location of the selectivity filter (in which histidine-201 adopts a central role) and diagrams of the NPA region may be found in also in these figures.[49]

To study the propensity for "open" and "closed" states along the lines of the "two-state" model (cf. Fig. 2, for example, configurations),[24,37] Fig. 3 depicts the probability distribution of d_{SF} and d_{CE} averaged over the four pores and sampled during both zero-field and statically applied field

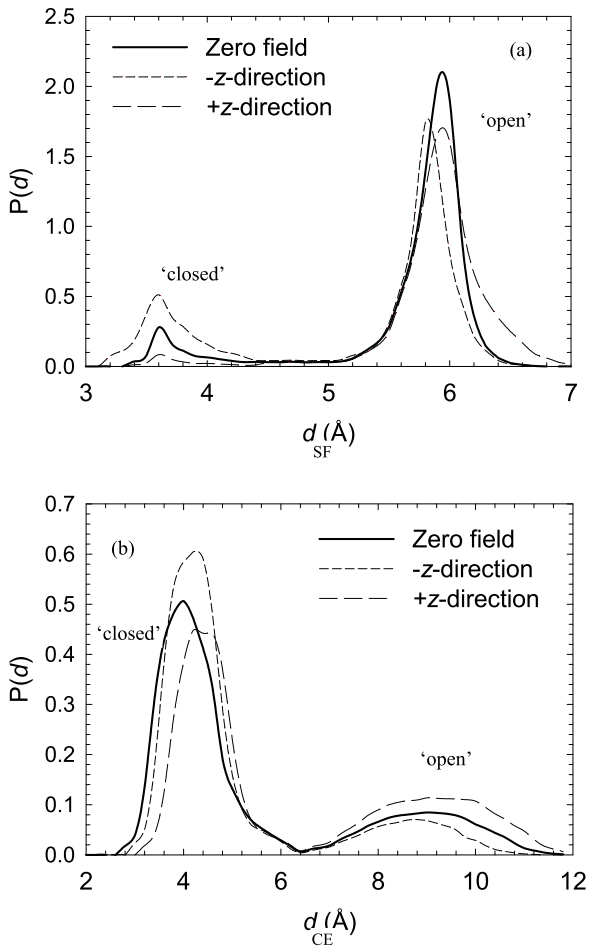

FIG. 3. Normalised probability distribution of (a) d_{SF} and (b) d_{CE} averaged over the four pores and sampled during zero-field conditions and for the static electric fields applied along the positive and negative z-directions.

conditions (along both $+z$ and $-z$-directions). It is readily apparent that for d_{SF}, this is open for the majority of the time in the zero (external)-field case. Of course, given that this (no-applied-field) state represents the protein *intrinsic* electric field of the experimental structure,[54] this intrinsic field points along the $+z$-axis (cf. Figs. 1(c) and 1(d)). Indeed, it was noted with some acuity in Ref. 24 that the d_{SF} distribution in that case overlaps with the experimental structure at $d_{SF} \sim 6$ Å for no manipulation of intrinsic electric field via ion placement on either side of the membrane, and we have a consistent finding here, with the SF open around 91% of the time. In terms of relative open/closed populations of CE, there is a much more delicate and even balance, demonstrating the rather decisive control on overall permeability exerted in this region (cf. Fig. 3(b)). For applied fields, Fig. 3(a) reveals a shift towards a greater degree of open states under $+z$-exposure for both SF and CE cases, in contrast to the opposite effect for fields along the $-z$-direction. In addition, the relative propensities for open and closed states in each of these critical regions are outlined in Table I, with the same clear trend as evident in Fig. 3 of a distinct bias towards more open states for +z-direction field exposure. Again, this is consistent with the findings of Ref. 24 in terms of applied potential (by ion-placement strategies on either side of the membrane, as opposed to a formally applied external electric field). Further, the self-diffusivity coefficients of water molecules passing through each channel (determined from the mean square displacement of those completing a passage therein)[49,50,76] showed an increase for periods of time where both parts of the pore were open and a decrease when both were closed, relative to the average value determined for the entire trajectory, and were slightly higher in the field applied along the $+z$-direction. In any event, the broad thrust of these findings is that externally applied static fields in this $+z$-direction serve to "open" the channel in the SF.

In a similar way, probability distribution of d_{SF} and d_{CE} averaged over the four pores in oscillating electric fields exhibits a suppression of open states for both cases for lower-frequency fields. This is particularly evident in Fig. 4, for 2.45, 20, and 100 GHz conditions (with two-state open-/close-propensities displayed in Table II for all oscillating-field conditions). Reversion towards zero-field behaviour (cf. Fig. 3) is clear for increasing frequency, with the 100 GHz results being essentially identical to the zero-field case. The motion of oscillating fields, turning back and forth along the $+z$ and $-z$ directions each half-period, *ipso facto*, shows that the greater propensity to close one or both regions for a (static) field applied along the $-z$-direction (cf. Fig. 3) more than "outweighs" the opening tendency exhibited by (static) fields

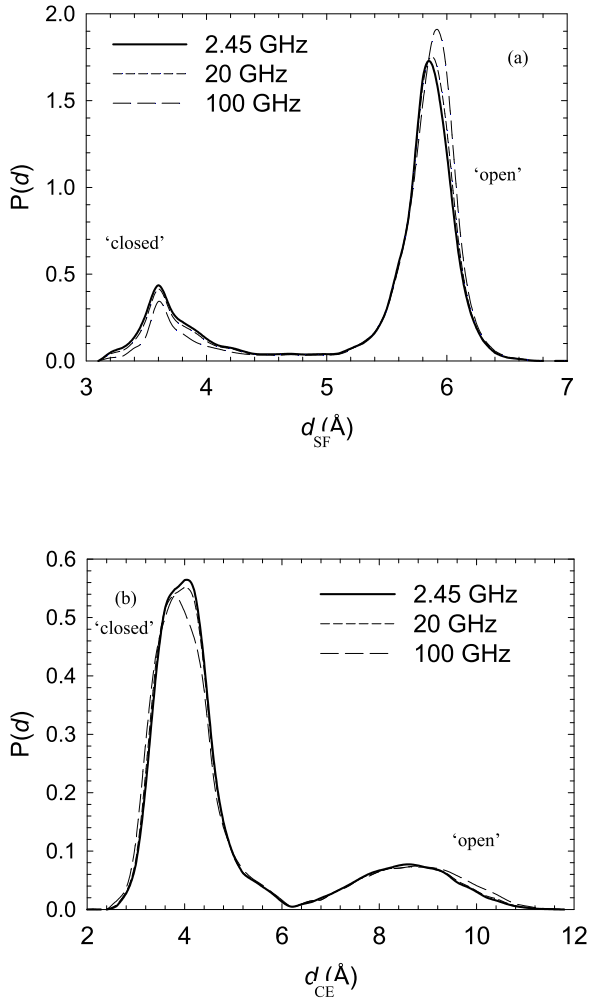

FIG. 4. Normalised probability distribution of (a) d_{SF} and (b) d_{CE} averaged over the four pores and sampled during 2.45, 20, and 100 GHz conditions. Reversion towards zero-field behaviour (cf. Fig. 3) is evident for increasing frequency.

acting along $+z$ (cf. Fig. 2), in the case of oscillating fields (cf. Fig. 4). This is particularly dramatic for 2.45 GHz, where the field period of ~0.41 ns results in half-periods along either $+z$- or $-z$-directions of the order of typical water-passage times through the pores. In this case, greater amplitude of partial realignment of residues' dipoles in each of these two regions was also observed *vis-à-vis* more rapidly oscillating fields, where there is insufficient time in each half-period to induce sufficient "distortion" of the pores to markedly change residue-dipolar alignment, open-/close-state populations, or

TABLE I. Proportion of time (%) for "open" ("o") and "closed" ("c") states of the selectivity-filter (SF) and CE regions, respectively, for the case of zero- and statically applied field conditions.

SF/CE	Zero field	$+z$-direction	$-z$-direction
o/o	23	35	15
c/o	~2	~3	~2
o/c	68	59	72
c/c	~7	~3	11

TABLE II. For axially applied time-varying external electric fields, the proportion of time (%) for "open" ("o") and "closed" ("c") states of the selectivity-filter (SF) and CE regions, respectively. Reversion towards zero-field behaviour (cf. Table I) is evident for increasing frequency.

SF/CE	2.45 GHz	20 GHz	50 GHz	100 GHz	200 GHz	500 GHz
o/o	11	14	15	17	19	22
c/o	9	6	~4	~4	~3	~2
o/c	68	70	71	70	67	68
c/c	12	10	10	9	11	~8

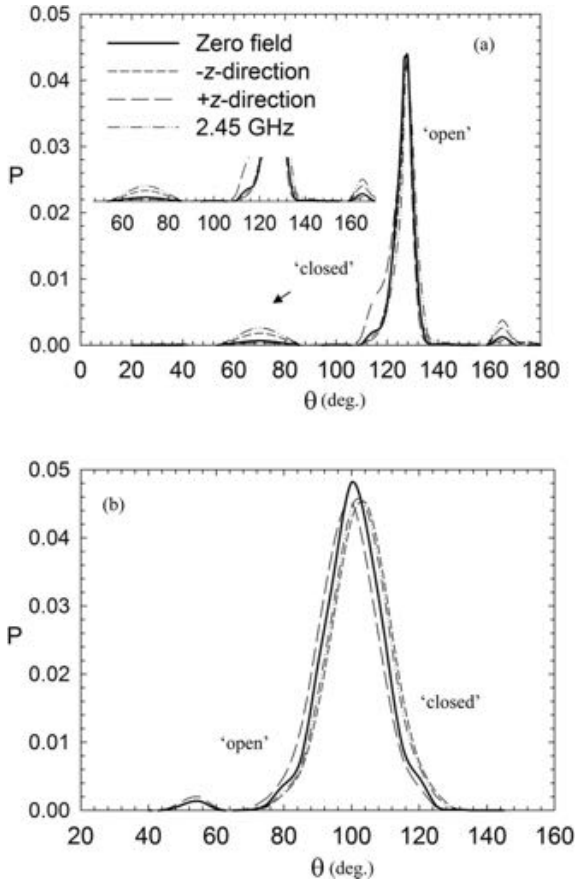

FIG. 5. Normalised probability distribution of θ (dipole vectors with respect to the +z-axis) for the (a) selectivity-filter (histidine-201) and (b) aromatic/arginine constrictive (histidine-95) regions averaged over the four pores and sampled during zero-field conditions and for the static electric fields applied along the positive and negative z-directions, as well as 2.45 GHz fields. The inset in (a) enlarges the "closed" states, showing greater propensity of 2.45 GHz to populate these. For (b), the notation is same as Fig. 3, and open and closed states overlap (cf. Figs. 3(b) and 4(b)). For (b), only zero-field and positive z-applied static field cases show the more open state at ~100°-125° w.r.t. the +z-axis.

water-passage dynamics. In particular, 2.45 GHz fields appear to shift towards a slightly greater propensity of SF and CE closure than static fields along the −z-axis.

To explore dipolar-alignment effects in both key regions more carefully, Fig. 5 depicts the probability distributions of angles between dipole vectors of both histidine-201 (part "(a)"—SF) and histidine-95 (part "(b)"—CE) with respect to the +z-axis—denoted as θ.[49,50] In particular, the insightful study of Alberga *et al.* in Ref. 37 has discussed the important potential role of histidine-95 in influencing the open versus closed status in the CE region, conjecturing how changes in environmental conditions could have an important effect thereon. Given the most dramatic effects have been observed for 2.45 GHz and static fields (cf. Figs. 3 and 4 and Tables I and II), these field conditions are shown in Fig. 5 (alongside the zero-field case). As determined before,[50] HIS-201 dipolar orientations adopt various distinct states (cf. Fig. 2). "Threshold" HIS-201 θ-values distinguish the configurations,[50] and these are: $\theta \gtrsim 130°$-135°, meaning marked dipolar alignment in a "open" state (typically with the external-field (instances) applied) along the +z-axis, as well as ~90° < θ < ~125°-130° (partial alignment and ostensibly/*de facto* "closed"), ~60° < θ < ~80° (essentially "closed"). The definitions of number of transitions between states were relatively robust with respect to small variations about approximate threshold values. Interestingly, the −z-aligned HIS-201 state of $\theta \gtrsim 165°$ was never observed in 100 ns zero-field simulations in Ref. 50 but is found very occasionally in the zero-field case for near-microsecond simulation (cf. Fig. 5(a) and also its inset)—indicating that the energy barriers can be traversed just occasionally by standard zero-field MD in longer-time simulations. As in Fig. 4 and Table II, the greater tendency of 2.45 GHz to shift to more closed states is evident. However, it is dramatic to note that the +z-applied static field leads to a very substantial "shoulder" in the θ_{201} distribution not evident for other field conditions, corresponding to the fully open states in d_{SF} in Fig. 3(a) for ~6-7 Å in the also-unique "shoulder" therein for +z-axis static fields.

In the case of θ_{95} in the CE region (HIS-95), the open and closed states overlap. Only zero-field and +z-applied static field cases exhibited the more open state at ~60°-100° relative to the +z-axis. However, there is a "shifting" of the distribution towards the more open state for +z-field cases (and towards more closed states for −z-field and low-frequency oscillating-field cases). The somewhat less dramatic, but still compelling, dipolar coupling of HIS-95 compared to HIS-201 in external fields owes in part to a larger-magnitude dipole of HIS-201 (~typically by ~13%-18%) and a somewhat more rigid local environment in the CE region. In any event, it is clear that the interplay of the intrinsic, physiological, and externally applied fields for the +z-applied static-field exposure leads to a bias in favour of enhanced mechanistic HIS dipolar alignment, which drives fundamentally the "stretching" of d_{SF} and d_{CE} witnessed in Figs. 3 and 4 towards a greater propensity of more open gating states.

Having established fundamental mechanistic details of dipolar coupling and populations of the two-state/two-region dichotomy, the natural and crucial matter of *directional* axially applied field effects on the free-energy landscape comes to the fore, in the guise of PMFs. In Ref. 50, this was determined precisely from metadynamics relative to the HIS-201 dipolar-dihedral angle $\angle C - C_\alpha - C_\beta - C_\gamma$, for the zero-field case and for two lower-intensity static-field exposures along the −z-axis; these data are reproduced in Fig. 6, along with the present study's results along the +z-axis. We have chosen HIS-201 dihedral alignment for consistency with Ref. 50 and also due to the key and exquisite "control" in shifting between overall-channel open and closed states (cf. Figs. 3(a) and 5(a) with approximate 85%-90% versus 10%-15% ratios in favour of open), and the more sensitive nature of HIS-201 angular dipolar-alignment *vis-à-vis* HIS-95 in response to applied fields (cf. Fig. 5(a) vs. 5(b)). The zero-field profile (cf. Fig. 6(a)) has two minima, at 70° and 150°. A ~5 kcal/mol barrier separates these, hindering "proper" sampling along this reaction coordinate (alleviated somewhat, but hardly satisfactorily, by near-microsecond "direct" MD). In addition, a shallow local minimum located at −50° is observed. As argued,[50] this is in line with Ref. 49, where only the former two states are visited. As found in Ref. 50, the −z-axis

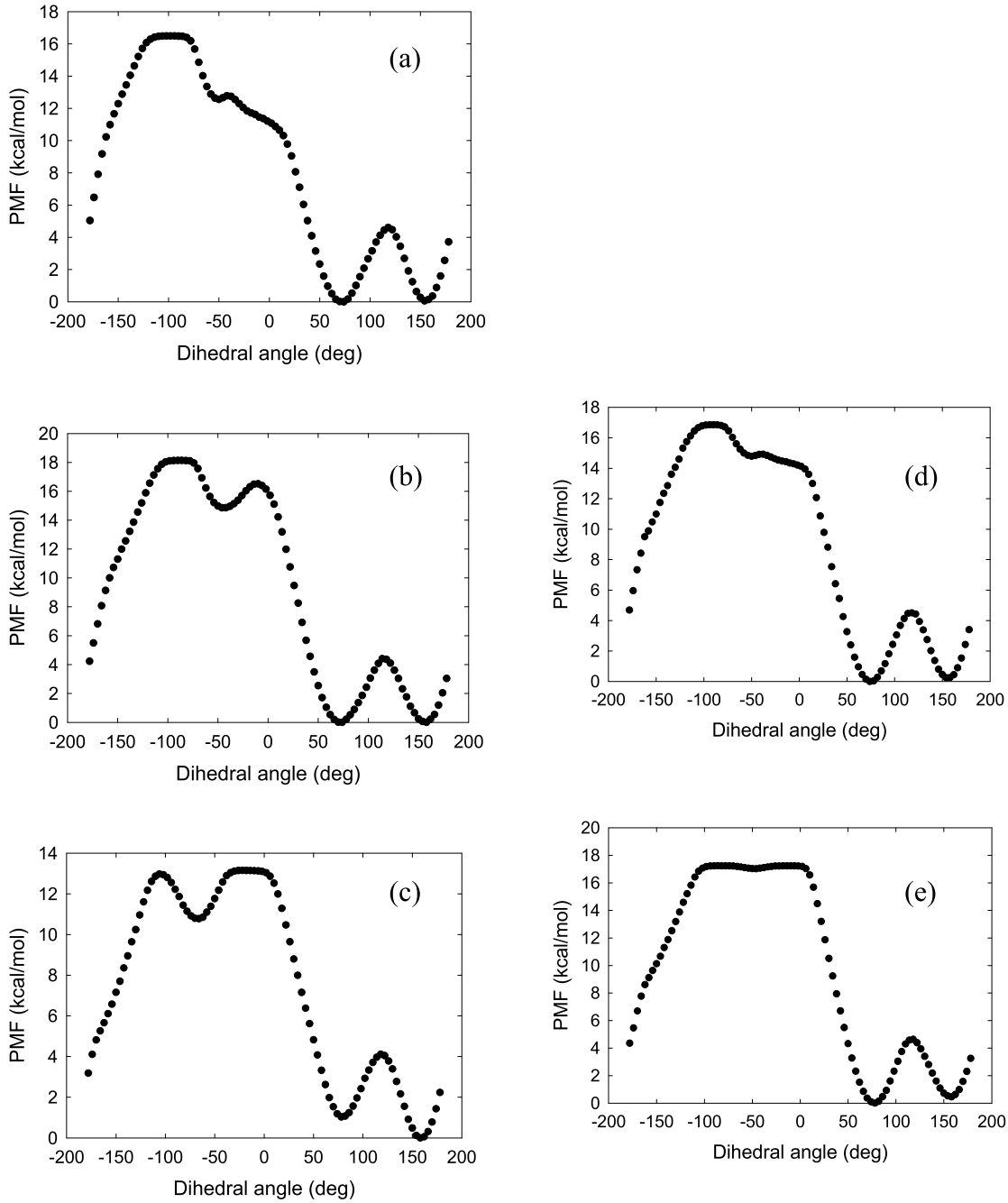

FIG. 6. Zero-set-minimum potential-of-mean-force (PMF) profiles determined from metadynamics with the collective variable as the HIS-201 dihedral angle. (a) Zero-field; (b) and (c) static fields of one-tenth and half-intensity, respectively, along the −z-axis; (d) and (e) static fields of one-tenth and half-intensity, respectively, along the +z-axis.

applied fields (on the left of Fig. 6, in parts (b) and (c)) switch the preference towards the 150° region, with a ΔG of −1.5 kcal/mol relative to the 70° region. Moreover, the barrier between these two states is slightly reduced. The previously observed minimum around the −50° area is more pronounced; however, the barriers are still similarly high. Remarkably, however, for +z-axis-applied fields (on the right, in parts (d) and (e)) depicts a dramatic "flattening" ((d), one-tenth intensity) and complete *removal* of barrier ((e), half-intensity) in and around the −50° region. Crucially, this removal of dihedral-"stretching" energy barrier in the more extensive locale surrounding the −50° region facilitates the more free sampling of the aggressively open HIS-201/d_{SF} states observed in Figs. 3(a) and 5(a) for the +z-applied fields (with the dramatic ~65°-75° and ~6-7 Å "shoulders"). Further, the +z-field PMFs on the right of Fig. 6 show only a mild switch in preference to the 70° region, with a ΔG of approximately −0.5 kcal/mol relative to the 150° area, with slight reduction in inter-minima barrier. Of course, these field effects depend on intensities, with one-tenth strengths having much less effect.

CONCLUSIONS

For axially applied static and oscillating electric fields, in-pore gating dynamics was studied in h-AQP4 via near-

microsecond NEMD, along with in-field metadynamics, particularly of the relative propensities for "open" and "closed" states of the conserved arginines in the arginine/aromatic constrictive area. In such a manner, the intimate connection of field-response governing "two-state" histidine states was established statistically and mechanistically. Direct measurement of deterministic MD in conjunction with applied-field metadynamics found that the *intrinsic* electric field within the pore points along the $+z$-axis, such that externally applied static fields in this direction served to "open" the channel in both the selectivity-filter and CE regions. This was found to be especially important for dipolar alignment of HIS-201 in the SF region, and also for HIS-95 in the CE region. In particular, the removal of the free-energy barrier for HIS-201-dihedral sampling of aggressively open configurations was determined to have a decisive, mechanistic impact in governing this process. In a sense, this study builds upon aspects of the very insightful and interesting earlier works of Hub *et al.*[24] and Alberga *et al.*,[37] by confirming electric-potential effects on the two-state/two-region paradigm and confirming the importance of the CE region and HIS-95 in regulating gating dynamics, whilst also tackling open questions left outstanding from our previous studies of Refs. 49 and 50, in the area of axial-field directionality and the interplay of intrinsic and external potentials of the same magnitude, with the –z-applied static field effectively "cancelling out" the zero-field intrinsic, electric field. Interestingly, the normal transmembrane potential ranges from −80 to −40 mV; thus, a field oriented towards the cell interior is generated. In this way, the tendency for the channel to be more closed under the effects static fields applied in the −z direction (akin to normal physiological conditions) seems to be the "default setting" for h-AQP4. Also, although not considered in detail in this study, owing to the emphasis on the two-state/two-region model,[24] Alberga *et al.*[37] have highlighted the importance of CYS-178 and pore-mouth regions in general for water passage; we have considered electric-field effects on CYS-178 (and others) recently.[77]

In future, it would be interesting to probe via metadynamics, using dipolar orientation of key residues as a collective variable, e.g., HIS-95 and 201 (or, indeed, CYS-178)—the dihedral angle used here and in Ref. 50 is not a perfect proxy for the dipole in the case of HIS-201 (and other residues, more generally). Recent work is encouraging in this regard[78,79] in rendering this more feasible in the near- to medium-term. Another key intriguing, titillating, possibility relates to using mutation of key residues in aquaporins to regulate and control gating dynamics and water permeability.[80] MD may offer scope for rigorous *predictive* determination of such key mutation strategies for subsequent *in vitro* studies; external electric fields may offer a convenient operational-control strategy for such efforts.

ACKNOWLEDGMENTS

N.J.E. thanks Science Foundation Ireland (Grant No. 15/ERC/I3142), and also the Irish Centre for High-End Computing and PRACE-DEISA Tier 1 (Cineca) for the provision of High-Performance Computing facilities. J.-A.G. acknowledges financial support from the Programa de Financiamiento Basal PFB16 Fundación Ciencia & Vida and ICM-ECONOMIA P09-022-F. N.J.E. thanks Paolo Marracino, Francesca Apollonio, and Micaela Liberti for interesting discussions. J.-A.G. thanks Yerko Escalona for help in electrostatic-potential calculations.

[1]S. Hohmann, S. Nielsen, and P. Agre, *Aquaporins* (Academic Press, San Diego, 2001).
[2]M. Borgnia, S. Nielsen, A. Engel, and P. Agre, Annu. Rev. Biochem. **68**, 425 (1999).
[3]L. S. King, D. Kozono, and P. Agre, Nat. Rev. Mol. Cell Biol. **5**, 687 (2004).
[4]G. M. Preston, P. Piazza-Carroll, W. B. Guggino, and P. Agre, Science **256**, 385 (1992).
[5]A. Engel and H. Stahlberg, Int. Rev. Cytol. **215**, 75 (2002).
[6]A. Finkelstein, *Water Movement Through Lipid Bilayers, Pores, and Plasma Membranes* (John Wiley & Sons, New York, 1987).
[7]G. Calamita, "The *Escherichia coli* aquaporin-z water channel," Mol. Microbiol. **37**, 254 (2000).
[8]M. J. Borgnia, D. Kozono, G. Calamita, P. C. Maloney, and P. Agre, J. Mol. Biol. **291**, 1169 (1999).
[9]Y. Fujiyoshi, K. Mitsuoka, B. L. de Groot, A. Philippsen, H. Grubmüller, P. Agre, and A. Engel, Curr. Opin. Struct. Biol. **12**, 509 (2002).
[10]R. M. Stroud, D. Savage, L. J. W. Miercke, J. K. Lee, S. Khademi, and W. Harries, FEBS Lett. **555**, 79 (2003).
[11]B. L. de Groot, A. Engel, and H. Grubmüller, FEBS Lett. **504**, 206 (2001).
[12]H. Sui, B.-G. Han, J. K. Lee, P. Walian, and B. K. Jap, Nature **414**, 872 (2001).
[13]D. Fu, A. Libson, L. J. Miercke, C. Weitzman, P. Nollert, J. Krucinski, and R. M. Stroud, Science **290**, 481 (2000).
[14]B. L. de Groot and H. Grubmüller, Science **294**, 2353 (2001).
[15]E. Tajkhorshid, P. Nollert, M. Ø. Jensen, L. J. W. Miercke, J. O'Connel, R. M. Stroud, and K. Schulten, Science **296**, 525 (2002).
[16]M. Ø. Jensen, E. Tajkhorshid, and K. Schulten, Biophys. J. **85**, 2884 (2003).
[17]F. Zhu, E. Tajkhorshid, and K. Schulten, FEBS Lett. **504**, 212 (2001).
[18]F. Zhu, E. Tajkhorshid, and K. Schulten, Biophys. J. **83**, 154 (2002).
[19]F. Zhu, E. Tajkhorshid, and K. Schulten, Biophys. J. **86**, 50 (2004).
[20]M. Hashido, M. Ikeguchi, and A. Kidera, FEBS Lett. **579**, 5549 (2005).
[21]M. Hashido, A. Kidera, and M. Ikeguchi, Biophys. J. **93**, 373 (2007).
[22]M. Ø. Jensen and O. G. Mouritsen, Biophys. J. **90**, 2270 (2006).
[23]B. G. Han, A. B. Guliaev, P. J. Walian, and B. K. Jap, J. Mol. Biol. **360**, 285 (2006).
[24]J. S. Hub, C. Aponte-Santamaría, H. Grubmüller, and B. L. de Groot, Biophys. J. **99**, L97 (2010).
[25]B. L. de Groot, T. Frigato, V. Helms, and H. Grubmuller, J. Mol. Biol. **333**, 279 (2003).
[26]N. Chakrabarti, E. Tajkhorshid, B. Roux, and R. Pomes, Structure **12**, 65 (2004).
[27]N. Chakrabarti, B. Roux, and R. Pomes, J. Mol. Biol. **343**, 493 (2004).
[28]B. Ilan, E. Tajkhorshid, K. Schulten, and G. A. Voth, Proteins **55**, 223 (2004).
[29]H. Chen, Y. Wu, and G. A. Voth, Biophys. J. **90**, L73 (2006).
[30]B. L. de Groot and H. Grubmüller, Curr. Opin. Struct. Biol. **15**, 176 (2005).
[31]M. Ø. Jensen, E. Tajkhorshid, and K. Schulten, Structure **9**, 1083 (2001).
[32]M. Ø. Jensen, S. Park, E. Tajkhorshid, and K. Schulten, Proc. Natl. Acad. Sci. U. S. A. **99**, 6731 (2002).
[33]J. S. Hub and B. L. de Groot, Biophys. J. **91**, 842 (2006).
[34]J. Henin, E. Tajkhorshid, K. Schulten, and C. Chipot, Biophys. J. **94**, 832 (2008).
[35]H. Khandelia, M. Ø. Jensen, and O. G. Mouritsen, J. Phys. Chem. B **113**, 5239 (2009).
[36]N. Smolin, B. Li, D. A. C. Beck, and V. Daggett, Biophys. J. **95**, 1089 (2008).
[37]D. Alberga, O. Nicolotti, G. Lattanzi, G. P. Nicchia, A. Frigeri, F. Pisani, V. Benfenati, and G. F. Mangiatordi, Biochim. Biophys. Acta **1838**, 3052–3060 (2014).
[38]M. Ø. Jensen, R. O. Dror, H. Xu, D. W. Borhani, I. T. Arkin, M. P. Eastwood, and D. E. Shaw, Proc. Natl. Acad. Sci. U. S. A. **105**, 14430 (2008).
[39]G. T. Manley, M. Fujimura, T. Ma, N. Noshita, F. Filiz, A. W. Bollen, P. Chan, and A. S. Verman, Nat. Med. **6**, 159 (2000).
[40]J. D. Ho, R. Yeh, A. Sandstrom, I. Chorny, W. E. C. Harries, R. A. Robbins, L. J. W. Miercke, and R. M. Stroud, Proc. Natl. Acad. Sci. U. S. A. **106**, 7437 (2009).

[41]G. Y. Solomentsev, N. J. English, and D. A. Mooney, J. Comp. Chem. **33**, 917 (2012).
[42]N. J. English and D. A. Mooney, J. Chem. Phys. **126**(9), 091105 (2007).
[43]N. J. English, G. Y. Solomentsev, and P. O'Brien, J. Chem. Phys. **131**, 035106 (2009).
[44]G. Y. Solomentsev, N. J. English, and D. A. Mooney, J. Chem. Phys. **133**, 235102 (2010).
[45]N. J. English and C. J. Waldron, Phys. Chem. Chem. Phys. **17**, 12407 (2015).
[46]N. Todorova, A. Bentvelzen, N. J. English, and I. Yarovsky, J. Chem. Phys. **144**, 085101 (2016).
[47]R. Mulero, A. S. Prabhu, K. J. Freedman, and M. J. Kim, J. Lab. Autom. **15**, 243–252 (2010).
[48]K. H. Schoenbach, B. Hargrave, R. P. Joshi, J. F. Kolb, R. Nuccitelli, C. Osgood, A. Pakhomov, M. Stacey, R. J. Swanson, J. A. White, S. Xiao, and J. Zhang, IEEE Trans. Dielectr. Electr. Insul. **14**, 1088 (2007).
[49]J.-A. Garate, N. J. English, and J. M. D. MacElroy, J. Chem. Phys. **136**, 055110 (2011).
[50]R. Reale, N. J. English, J.-A. Garate, P. Marracino, M. Liberti, and F. Apollonio, J. Chem. Phys. **139**, 205101 (2013).
[51]J.-A. Garate, N. J. English, and J. M. D. MacElroy, Mol. Simul. **35**, 3 (2009).
[52]J.-A. Garate, N. J. English, and J. M. D. MacElroy, J. Chem. Phys. **131**, 114508 (2009).
[53]N. J. English, J.-A. Garate, and J. M. D. MacElroy, "Static and alternating electric field and distance-dependent effects on carbon nanotube-assisted water self-diffusion across lipid membranes," in *Carbon Nanotubes* (Intech, 2011).
[54]J. Gumbart, F. Khalili-Araghi, M. Sotomayor, and B. Roux, Biochim. Biophys. Acta **1818**, 294 (2012).
[55]F. C. Bernstein, T. F. Koetzle, F. C. Bernstein, T. F. Koetzle, G. J. Williams, E. F. Meyer, M. D. Brice, J. R. Rogers, O. Kennard, T. Shimanouchi, and M. Tasumi, J. Mol. Biol. **112**, 535 (1977).
[56]A. D. MacKerell, Jr., D. Bashford, M. Bellott, R. L. Dunbrack, Jr., J. Evanseck, M. J. Field, S. Fischer, J. Gao, H. Guo, S. Ha, D. Joseph, L. Kuchnir, K. Kuczera, F. T. K. Lau, C. Mattos, S. Michnick, T. Ngo, D. T. Nguyen, B. Prodhom, I. W. E. Reiher, B. Roux, M. Schlenkrich, J. Smith, R. Stote, J. Straub, M. Watanabe, J. Wiorkiewicz-Kuczera, D. Yin, and M. Karplus, J. Phys. Chem. B **102**, 3586 (1998).
[57]S. E. Feller and A. MacKerell, J. Phys. Chem. B **104**, 7510 (2000).
[58]W. Humphrey, A. Dalke, and K. Schulten, J. Mol. Graph. **14**, 33 (1996).
[59]J. C. Phillips, R. Braun, W. Wang, J. Gumbart, E. Tajkhorshid, E. Villa, C. Chipot, R. D. Skeel, L. Kale, and K. Schulten, J. Comput. Chem. **26**, 1781 (2005).
[60]W. L. Jorgensen, J. Chandrasekhar, J. D. Madura, R. W. Impey, and M. L. Klein, J. Chem. Phys. **79**, 926 (1983).
[61]T. Darden, D. York, and L. Pedersen, J. Chem. Phys. **98**, 10089 (1993).
[62]M. Tuckerman, B. J. Berne, and G. J. Martyna, J. Chem. Phys. **97**, 1990 (1992).
[63]G. J. Martyna, D. J. Tobias, and M. L. Klein, J. Chem. Phys. **101**, 4177 (1994).
[64]G. S. Grest and K. Kremer, Phys. Rev. A **33**, 3628 (1986).
[65]J. P. Ryckaert, G. Ciccotti, and H. J. C. Berendsen, J. Comput. Phys. **23**, 327 (1977).
[66]N. J. English and J. M. D. MacElroy, J. Chem. Phys. **119**, 11806 (2003).
[67]N. J. English, Mol. Phys. **104**, 243 (2006).
[68]D. L. Scovell, T. D. Pinkerton, V. K. Medvedev, and E. M. Stuve, Surf. Sci. **457**, 365 (2000).
[69]J. E. Stone, J. C. Phillips, P. L. Freddolino, D. J. Hardy, L. G. Trabuco, and K. Schulten, J. Comput. Chem. **28**(16), 2618–2640 (2007).
[70]N. J. English, Energies **6**, 3072 (2013).
[71]N. Varini, N. J. English, and C. Trott, Energies **5**, 3526 (2012).
[72]T. Huber, A. E. Torda, and W. F. van Gunsteren, J. Comput.-Aided Mol. Des. **8**, 695 (1994).
[73]A. Laio and M. Parrinello, Proc. Natl. Acad. Sci. U. S. A. **99**, 12562 (2002).
[74]N. J. English and J. M. D. MacElroy, J. Chem. Phys. **118**, 1589 (2003).
[75]F. Calvo and P. Dugourd, Biophys. J. **95**, 18 (2008).
[76]M. P. Allen and D. J. Tildesley, *Computer Simulation of Liquids* (Oxford, 1987).
[77]P. Marracino, M. Liberti, E. Trapani, C. J. Burnham, M. Avena, J.-A. Garate, F. Apollonio, and N. J. English, Int. J. Mol. Sci. **17**, 1133 (2016).
[78]Y. Escalona, N. J. English, T. Perez-Acle, and J.-A. Garate, "Gating thermodynamics of h-AQP4: Free-energy calculations of dipolar alignment along the selectivity filter in static electric fields," (in statu nascendi).
[79]A. Bernadin, C. Yañez, N. J. English, Y. Escalona, T. Perez-Acle, and J.-A. Garate, "Dipole alignment: A novel collective variable for harmonic restraining and free-energy calculations in NAMD," (in statu nascendi).
[80]P. Kitchen and A. C. Conner, Biochemistry **54**, 6753–6755 (2015).